Multi-elemental imaging of paraffin-embedded human samples by laser-induced breakdown spectroscopy

S. Moncayo, F. Trichard, B. Busser, M. Sabatier-Vincent, F. Pelascini, N. Pinel, I. Templier, J. Charles, L. Sancey, V. Motto-Ros

PII: S0584-8547(17)30077-0
DOI: doi: 10.1016/j.sab.2017.04.013
Reference: SAB 5246

To appear in: *Spectrochimica Acta Part B: Atomic Spectroscopy*

Received date: 10 February 2017
Revised date: 12 April 2017
Accepted date: 28 April 2017

Please cite this article as: S. Moncayo, F. Trichard, B. Busser, M. Sabatier-Vincent, F. Pelascini, N. Pinel, I. Templier, J. Charles, L. Sancey, V. Motto-Ros , Multi-elemental imaging of paraffin-embedded human samples by laser-induced breakdown spectroscopy, *Spectrochimica Acta Part B: Atomic Spectroscopy* (2016), doi: 10.1016/j.sab.2017.04.013

Multi-elemental imaging of paraffin-embedded human samples by laser-induced breakdown spectroscopy

S. Moncayo[a], F. Trichard[a], B. Busser[a,b,c], M. Sabatier-Vincent[b], F. Pelascini[d], N. Pinel[b], I. Templier[b], J. Charles[b,c], L. Sancey[c] and V. Motto-Ros[a]

[a] Institut Lumière Matière UMR 5306, Université Lyon 1 - CNRS, Université de Lyon 69622 Villeurbanne, France.

[b] Grenoble University Hospital, F-38000 Grenoble, France.

[c] Université Grenoble Alpes, Institute of Advanced Biosciences, IAB INSERM U1209 CNRS UMR5309, F-38000 Grenoble, France.

[d] CRITT Matériaux Alsace, 67305 Schiltigheim, France.

Corresponding author: vincent.motto-ros@univ-lyon1.fr

Abstract:

Chemical elements play central roles for physiological homeostasis in human cells, and their dysregulation might lead to a certain number of pathologies. Novel imaging techniques that improve the work of pathologists for tissue analysis and diagnostics are continuously sought. We report the use of Laser-Induced Breakdown Spectroscopy (LIBS) to perform multi-elemental images of human paraffin-embedded skin samples on the entire biopsy scale in a complementary and compatible way with microscope histopathological examination. A specific instrumental configuration is proposed in order to detect most of the elements of medical interest (i.e. P, Al, Mg, Na, Zn, Si, Fe, and Cu). As an example of medical application, we selected and analysed skin biopsies, including healthy skin tissue, cutaneous metastasis of melanoma, Merkel-cell carcinoma and squamous cell carcinoma. Clear distinctions in the distribution of chemical elements are observed from the different samples investigated. This study demonstrates the high complementarity of LIBS elemental imaging with conventional histopathology, opening new opportunities for any medical application involving metals.

Keywords: LIBS Imaging, elemental imaging, human paraffin-embedded tissue, Skin cancer

1. Introduction

Great interest has recently aroused in the study of the dysregulation of chemical elements within tissues [1-3]. The distribution of elements in biological tissues is an important source of information that can contribute to the diagnostic and therapeutic procedures [4,5] as for example, in case of skin cancer, the most common form of cancer in Europe and the United States [6,7]. For a better understanding of their role in biological mechanisms such as metal transport, storage, and distribution, the identification and quantification of the metals, directly in their native physiological environment in tissues is always sought [8]. In histology laboratories, the pathologist might opt for an approach named chromogenic detection that requires the use of stains and indicators. This procedure is usually applied in daily routine for the detection of metals in biological tissues. However, the chromogenic method suffer from several limitations (long preparation consuming, poor sensitivity, only one element detected at the same time, limited to certain metals) [9] and tends to be replaced by more sensitive analytical methods such as transmission electron microscopy combined with energy dispersive X-ray analysis (TEM-EDX) [10,11], synchrotron radiation microanalysis (SXRF) [12-14] or laser ablation inductively coupled plasma spectrometry mass spectrometry (LA-ICP-MS) [15-18]. Although these techniques offer high performance in terms of sensitivity and/or spatial resolution, the complexity of the required equipment along with their relatively slow analysis, make their use rather restrictive and difficult for routine medical diagnosis. These approaches require in addition specific sample preparation that may hinder the analysis of paraffin-embedded specimens and so limit their complementarity with conventional histopathology procedures, which involve formalin fixation and paraffin embedding (FFPE) and preparation of hematoxylin and eosin stained (HES) sections for microscopic optical evaluation. Although different fixation procedure can be used, FFPE approach has emerged as the worldwide gold standard, in the sense that the large majority of human biopsies are stored in paraffin. For the first time, to the best of our knowledge, we evaluated the use of Laser Induced Breakdown Spectroscopy (LIBS) [19,20] to obtain elemental images of paraffin-embedded human biopsies of healthy and malignant skin tissues in a complementary manner with histopathology analysis. In LIBS imaging, laser-induced plasma are produced continuously while scanning the sample surface over the region of interest. Elemental images are obtained after extracting the intensity of the interesting species (i.e. atoms or ions) from each recorded spectrum [21,22]. This technology provides significant advantages over the other approaches, such as working at atmospheric pressure, speed of operation (up to 100 Hz), ease of use, and full compatibility with optical

microscopy, and therefore with conventional histopathology. Our previous works demonstrated state of the art results in the bioelemental imaging of exogenous metal in mice organ, with typical spatial resolution of 10 µm and a sensitivity level at the ppm scale [11, 23-28]. In all these previous studies, biological organs were fixed in epoxy resin. This is a conventional protocol for electron microscopy experiments that allows to embed the tissue in a hard form to ensure the best ablation efficiency for LIBS. In medicine, the analysis of paraffin-embedded samples is indispensable to be completely compatible with conventional pathological procedure and so to allow a direct comparison with HES sections. The direct analysis of human paraffin-embedded tissues is however challenging from a technical point of view, since it involves mastering the laser ablation of soft material and the difficulty to obtain reliable elemental images of endogenous elements at low physiological concentration levels with micrometer spatial resolution over large biopsies surfaces (~12 cm^2).

This paper demonstrates for the first time the applicability of LIBS imaging for analysing paraffin-embedded human skin biopsies, including healthy skin tissue, cutaneous metastasis of melanoma, Merkel-cell carcinoma and squamous cell carcinoma. A dedicated instrumental configuration is proposed, allowing to detect the most meaningful metal and non-metal elements in medical applications (P, Cu, Zn, Fe, Al, Mg, Na, Si). Differences in the content and the spatial distribution of the chemical elemental within tumours were found and may offer a new strategy for the study, diagnosis and staging of skin cancer. More generally, this work represent the first step towards the implementation of LIBS imaging technique in clinical diagnosis laboratories for multiple medical applications.

2. Experimental methods

The human biopsies all came from formalin-fixed, paraffin-embedded (FFPE) archived material stored in the pathology department from Grenoble University Hospital. All the patients signed informed consent, and the clinical procedure was approved by a local ethics committee (Prof J. Charles, CPP Sud-Est). For this work, healthy skin tissue came from a female patient who underwent reduction mammoplasty. We also selected 3 biopsies from patients suffering from metastatic melanoma, Merkel-cell carcinoma (MCC) and squamous cell carcinoma (SCC). Metastatic melanoma is not a common cancer. However, it is incurable because of its quick metastasis to other parts of the body [29]. MCC is an unusual but highly aggressive skin cancer mainly developed in elderly people, whose diagnosis is generally not well established and could be mistaken with

other malignant pathologies [30]. Finally, SCC is the second most common form of skin cancer; once these tumours have recurred or metastasized, disease control is often difficult and survival rates are poor [31]. For each paraffin block sample, a 5 µm-thick slice was stained with Haematoxylin-Eosin-Saffron (HES), and the adjacent paraffin block was further analysed by LIBS allowing its direct comparison.

A schematic representation of the LIBS instrumentation is shown in Fig. 1a. Briefly, we used a Nd:YAG laser emitting 5 ns pulses at the fundamental wavelength (1064 nm) with a 10 Hz repetition rate. Laser pulses were vertically focused onto the sample surface by a 15x magnification reflective objective (LMM-15X-P01, Thorlabs), and the plasma emission was collected by two lens-fibre systems coupled to two independent Czerny-Turner spectrometers used to cover the spectral ranges required for the simultaneous detection of all the elements of interest. For the detection of Fe, Mg, Na, Ca, Al, Cu, and Si, a Shamrock 500 (Andor technology) equipped with a grating of 600 l/mm, an ICCD camera of 2048x512 pixels, and a 25 mm intensifier covering a spectral range of approximately 80 nm (270-340 nm) was used, and secondly, a Shamrock 303 (Andor technology) with a grating of 1200 l/mm and an ICCD camera dedicated to the UV range covering a spectral range of approximately 40 nm (190-230 nm), was used for the detection P and Zn. The spectral resolution was approximately 0.15 nm for both spectrometers. Both ICCD cameras were synchronized to the Q-switch of the laser, and acquisitions were performed with the typical delay and gate of 1000 ns and 5 µs, respectively. An argon flow (1.5 l/min) blowing through the plasma was used both to prevent surface contamination by ablated material deposition of the previous laser shots and to obtain a better sensitivity due to a better plasma confinement [32] that compensated the low ablation efficiency of such soft tissue.

Before conducting LIBS analysis, a thin slice of the paraffin bloc (5 µm) was collected and prepared for HES with conventional clinical tools. An example of HES image, obtained with a high-resolution scanner, is shown in Fig. 1b. This image represents two sections of the same biopsied tissue both fixed in the same bloc of paraffin. After, LIBS analysis was conducted directly on the bloc of paraffin, on a tissue section adjacent to the HES slice. As an example, five LIBS single shot spectra of skin biopsy tissue from different physiological areas are shown in Fig. 1c; the position of each spectrum is related to the HES image by a number from 1 to 5. Considering the actual laser repetition rate (10 Hz) and the step size (i.e. 50µm), the typical time to conduct the biopsy analysis (~ 3 cm^2) was approximately 3 hours per sample. To reduce the tissue damage

resulting from ablation, the laser pulse energy and its focalization onto the sample were strictly controlled [33], the energy for laser ablation was set and kept during the entire experiment at 2 mJ. To create images of the elements of interest, a previously developed spectral data treatment [23] was applied to extract the signal intensity. The algorithm detected given peaks and defined a polynomial function as the baseline. Afterward the emission signal was stored in a matrix where each cell contained the emission intensity at each sampling position for a given element. This matrix could then be displayed as an image by using a false colour scale. An example of elemental images is shown in Fig. 1d for Na, P, Mg, Fe, and Ca.

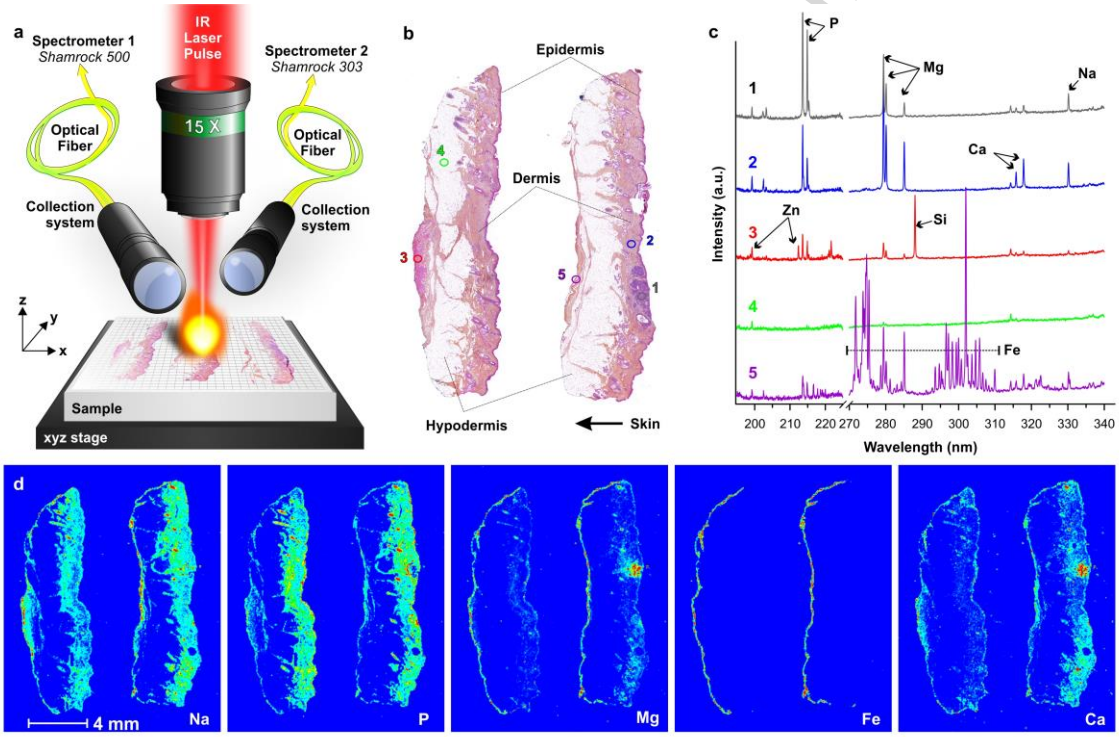

Fig. 1. Overview of LIBS imaging technology. (a) Schematic representation of the main components of the LIBS imaging instrument: a microscope objective to focus the laser pulse, a motorized sample stage and two optical detection systems coupled with two Czerny-Turner spectrometers. (b) High-resolution HES histological images of a healthy skin sample before LIBS analysis, (c) Typical single shot tissue spectrum covering the 270-340 nm for detecting Mg, Si, Fe, Cu, Al and Na, and the 190-230 nm detecting P and Zn on different areas of the tissue biopsy. (d) Na, P, Mg, Fe, and Ca LIBS images for a paraffin-embedded skin tissue.

3. Results and discussion

3.1 Healthy skin tissue

The results of the LIBS imaging on healthy tissue are shown in Fig. 2. The three layers forming the skin (*i.e.*, epidermis, dermis and hypodermis) can be easily identified after conventional HES staining. The epidermis is the most superficial layer of the skin and is responsible for protecting the body from harmful influences from the environment. It is visible as the darkest external layer on the HES image. The dermis is shown as a thicker pale pink layer. It is responsible for thermoregulation and for providing vital nutrients to the epidermis. Finally, the hypodermis is the deepest layer of the skin and is mainly composed of adipose tissue that is colourless after HES staining. This layer also helps in the regulation of body temperature and serves as an energetic reservoir. The associated LIBS elemental images are displayed with a cold-to-warm colour scale. They represent 140 800 (320 x 440) individual spectra that were recorded in approximately 3 hours. A strong heterogeneity of the elements in the skin is observed, and a comprehensive analysis of the elemental distributions allowed proper identification and discrimination of the three different physiological skin layers. The compatibility of LIBS and histopathological analysis allows identification of all of the physiological skin structures by a simple superimposition of the elemental image with those described by the pathologists after microscopy analysis of the HES-stained samples. In the hair follicle, we noticed a strong signal of most of the elements compared with that of the skin tissue; this result is in accordance with a study that reported the presence of tens of ppm of Mg, Ca, K, and Na in hairs [34].

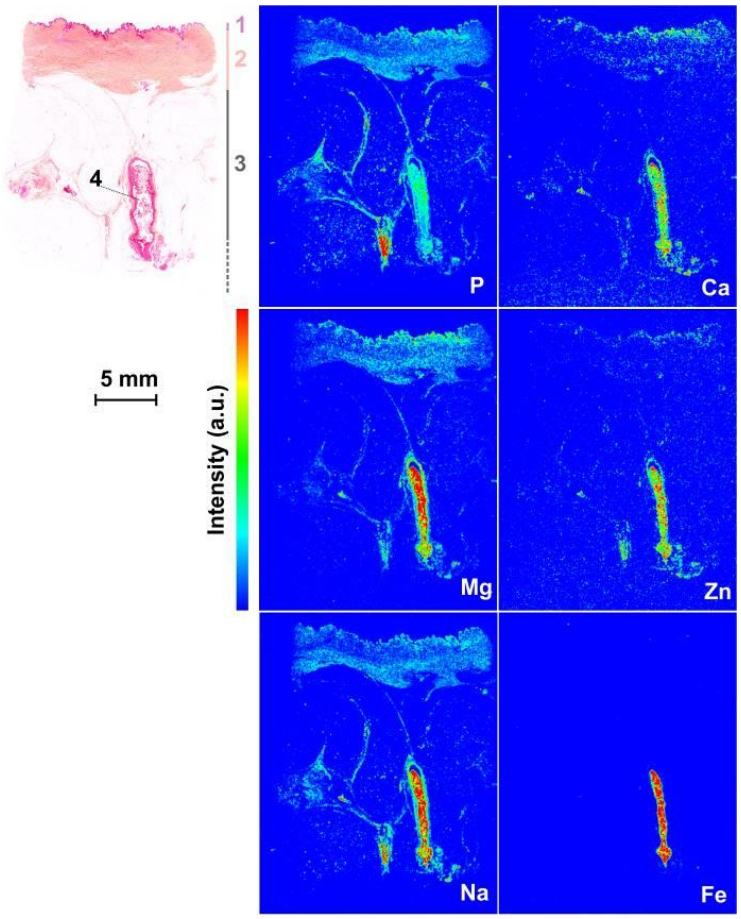

Fig. 2. Elemental imaging of healthy tissue. Left panel: HES staining image of a healthy skin sample with annotated skin physiological layers; epidermis, dermis and hypodermis are indicated by 1, 2 and 3, respectively. A hair follicle is also visible in both the HES and elemental images and is indicated by the number 4. Right panel: elemental images of P, Mg, Na, Ca, Zn and Fe (320 x 440 pixels, step size of 50 µm). The colour intensity scale of the different elemental images is expressed in arbitrary units.

3.2 Tumour tissues

The images of LIBS elemental analysis of three biopsies affected by three different skin cancer pathologies are shown in Fig. 3. With the aim of finding differences in the elemental distribution related to skin diseases, we investigated samples of human skin containing either a subcutaneous melanoma metastasis, MCC or SCC. Since the experimental parameters remained constant during all of the measurements and are displayed with the same intensity scales, all the elemental images are strictly comparable. Clear differences were found in the elemental distribution among the different types of tumour samples. As found for healthy skin, Ca, P, Na, and Mg are also present in skin cancers (Fig. 3). High levels of P, elemental indicator of cell nucleus, were

observed in all of the tumour areas. This fact is in accordance with the literature, since tumours are generally described as high cellular density areas after HES staining, because of the fast and uncontrolled growth of cancer cells [35].

In the case of the metastatic melanoma, the elemental images of the tumour revealed a concentration gradient for Ca, P, and Mg. This finding is in contrast with the apparent homogeneous pattern of the tumour cells after HES analysis. Similarly, in the MCC, we noticed higher concentrations of Ca and Zn in the region closest to the tumour; the concentration decreased with distance away from the tumour. Finally, in the SCC, the signals of Na, P, Mg, and Zn were stronger in the left area of the tumour and were lower in the right nodular part. These observations are in contrast with the Ca signal that appeared stronger in the right area. The external skin region was composed of most of the elements, *i.e*. Na, Mg, Ca, P, and Zn. The presence of blood (or large vessels) was evidenced with high levels of Fe, such as in the bottom areas of the SCC or MCC. In addition, very high concentrations of Fe, Cu, Ca, and Zn are visible in the lateral periphery of some tissues. This observation is related with the routine use of coloured inks in the process of skin biopsy samples in the pathology department. The ink staining reveals the proper orientation of the sample for the pathologist. As an example, green ink contained high amounts of Cu, whereas blue ink contained high levels of Zn and Fe. The ink residual signal does not represent a source of contamination and/or interference since it is always located in the border of the tissue, far from the regions of interest. The physiological parts of the skin, *i.e*., epidermis, dermis, and hypodermis were clearly identifiable in the tumour skin biopsies after analysis of several elemental images. These results show a different distribution and concentration of several elements between the tumours and the surrounding non-tumour tissue. The LIBS elemental images also allowed to visualize strong heterogeneities in the elemental distribution inside the tumour tissue, even within areas considered homogenous in histopathology analysis. We also noticed the presence of large dynamic concentration ranges for elements such as Ca, Na, Mg and Fe, with distinct areas presenting from low to high concentrations of these given elements.

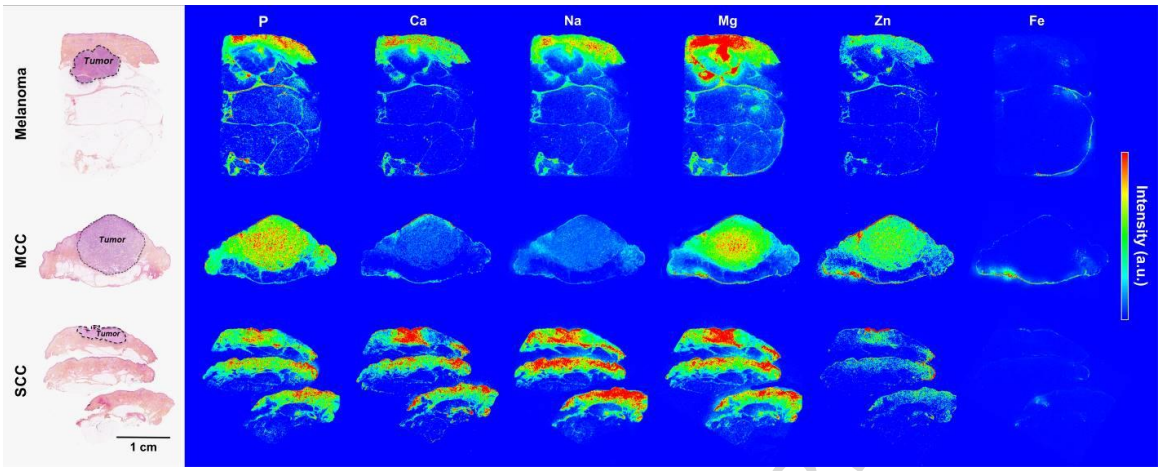

Fig. 3. Elemental imaging of different skin cancer types. Left panels: histological picture of the three studied skin cancer types after HES staining (melanoma metastasis, Merkel-cell carcinoma (MCC) and squamous cell carcinoma (SCC)). The different skin layers, *i.e.*, epidermis, dermis, and hypodermis are indicated and the dashed line indicates the tumour region. Right panels: elemental distributions of Ca, P, Na, Mg, Zn, and Fe are shown in a cold-to-warm colour scale (a.u. arbitrary units).

4. Conclusion

We developed and evaluated a novel methodology for elemental imaging of FFPE samples of human origin based on LIBS. In the proposed configuration, LIBS technology is completely compatible with the conventional pathological sample preparation procedures and allows the bio-distribution of elements of interest to be obtained in their native physiological environment. The elemental images performed on skin tissues allowed visualization and identification of the three physiological layers of the skin matching perfectly with the expected architecture and organization of the tissue by direct comparison with microscope pathological examination after HES staining. The elemental images of different tumours allowed characterization of the lesions, observing heterogeneous distributions of elements within areas that looked homogeneous after the pathological examination. Importantly, although we managed to perform the analysis of the elemental distribution of large-sized samples in about 3 hours of analysis per sample, the current upgrade of our instrument to 100 Hz laser repetition rate will help to reduce the analytical time by 10x (*i.e.* 18 min for similar large-sized samples).

The direct comparison between elemental and histopathological images of any tissue/sample of medical interest also allows the relation of the presence/absence of certain elements, in particular physiological

regions that could be associated with certain pathologies, bringing information beyond the visual histopathology. Altogether, this study demonstrated the great potential of LIBS imaging for contributing to a better understanding of the biology of the diseases and helping pathologists in their daily medical routine to improve medical diagnoses. In addition, future studies with an increased number of samples, are being carried out to provide new clues of the role of chemical elements during skin carcinogenesis and to enhance the statistical support toward to a greatest impact on clinical practice.

Acknowledgements

This work was partially supported by Pulsalys, the French Alsace Région and the research funds of the Institut Français National contre le Cancer and the INSERM within the project LAST (#PC201513).

References

[1] L. Rinaldi, G. Barabino, J.P. Klein, D. Bitounis, J. Pourchez, V. Forest, D. Boudard, L. Leclerc, G. Sarry, X. Roblin, M. Cottier, J.M. Phelip, Metals distribution in colorectal biopsies: New insight on the elemental fingerprint of tumour tissue, Digest Liver Dis, 47 (2015) 602-607.

[2] A. Al-Ebraheem, E. Dao, K. Geraki, M.J. Farquharson, Emerging Patterns in the Distribution of Trace Elements in Ovarian, Invasive and In-Situ Breast Cancer, J Phys: Conf Ser, 499 (2014) 012014.

[3]. M. Urszula, B. Dariusz, B. Janusz, G. Stanisław, K.-K. Aldona, K. Marek, Trace element concentration distributions in breast, lung and colon tissues, Phys Med Biol, 52 (2007) 3895.

[4] Y. Koga, T. Satoh, K. Kaira, M. Koka, T. Hisada, J. Hirato, B. Altan, M. Yatomi, A. Ono, Y. Kamide, Y. Shimizu, H. Aoki-Saito, H. Tsurumaki, K. Shimizu, A. Mogi, T. Ishizuka, M. Yamada, K. Dobashi, Elemental and immunohistochemical analysis of the lungs and hilar lymph node in a patient with asbestos exposure, a pilot study, Environ Health Prev Med, (2016) DOI: 10.1007/s12199-016-0576-5.

[5] A.A. Skalny, A.A. Tinkov, Y.S. Medvedeva, I.B. Alchinova, M.Y. Karganov, O.P. Ajsuvakova, A.V. Skalny, A.A. Nikonorov, Zinc asparaginate supplementation induces redistribution of toxic trace elements in rat tissues and organs, Interdiscip Toxicol, 8 (2015) 131-138.

[6] A.C. Society, Cancer Figures & Facts, American Cancer Society, Atlanta, 2016.

[7] H.J. Schulze, B. Cribier, L. Requena, J. Reifenberger, C. Ferrándiz, A. Garcia Diez, V. Tebbs, S. McRae, Imiquimod 5% cream for the treatment of superficial basal cell carcinoma: results from a randomized vehicle-controlled phase III study in Europe, Brit J Dermatol, 152 (2005) 939-947

[8] R. McRae, P. Bagchi, S. Sumalekshmy, C.J. Fahrni, In Situ Imaging of Metals in Cells and Tissues, Chem Rev, 109 (2009) 4780-4827.

[9] I. Susnea, R. Weiskirchen, Trace metal imaging in diagnostic of hepatic metal disease, Mass Spectrom Rev, 35 (2016) 666-686.

[10] W. Rima, L. Sancey, M.T. Aloy, E. Armandy, G.B. Alcantara, T. Epicier, A. Malchere, L. Joly-Pottuz, P. Mowat, F. Lux, O. Tillement, B. Burdin, A. Rivoire, C. Boule, I. Anselme-Bertrand, J. Pourchez, M. Cottier, S. Roux, C. Rodriguez-Lafrasse, P. Perriat, Internalization pathways into cancer cells of gadolinium-based radio sensitizing nanoparticles, Biomaterials, 34 (2013) 181-195.

[11] S. Kunjachan, A. Detappe, R. Kumar, T. Ireland, L. Cameron, D.E. Biancur, V. Motto-Ros, L. Sancey, S. Sridhar, G.M. Makrigiorgos, R.I. Berbeco, Nanoparticle Mediated Tumor Vascular Disruption: A Novel Strategy in Radiation Therapy, Nano lett, 15 (2015) 7488-7496.

[12] W. Chao, B.D. Harteneck, J.A. Liddle, E.H. Anderson, D.T. Attwood, Soft X-ray microscopy at a spatial resolution better than 15 nm, Nature, 435 (2005) 1210-1213.

[13] A. Sakdinawat, D. Attwood, Nanoscale X-ray imaging, Nat Photon, 4 (2010) 840-848.

[14] W. Meyer-Ilse, D. Hamamoto, A. Nair, S.A. Lelievre, G. Denbeaux, L. Johnson, A.L. Pearson, D. Yager, M.A. Legros, C.A. Larabell, High resolution protein localization using soft X-ray microscopy, J Microsc, 201 (2001) 395-403.

[15] J.S. Becker, M. Zoriy, A. Matusch, B. Wu, D. Salber, C. Palm, J.S. Becker, Bioimaging of metals by laser ablation inductively coupled plasma mass spectrometry (LA-ICP-MS), Mass Spectrom Rev, 29 (2010) 156-175.

[16] J.S. Becker, M.V. Zoriy, C. Pickhardt, N. Palomero-Gallagher, K. Zilles, Imaging of copper, zinc, and other elements in thin section of human brain samples (hippocampus) by laser ablation inductively coupled plasma mass spectrometry, Anal Chem, 77 (2005) 3208-3216.

[17] E. Moreno-Gordaliza, C. Giesen, A. Lázaro, D. Esteban-Fernández, B. Humanes, B. Cañas, U. Panne, A. Tejedor, N. Jakubowski, M.M. Gómez-Gómez, Elemental Bioimaging in Kidney by LA–ICP–MS As a Tool to Study Nephrotoxicity and Renal Protective Strategies in Cisplatin Therapies, Anal Chem, 83 (2011) 7933-7940.

[18] M. Bonta, J.J. Gonzalez, C.D. Quarles, R.E. Russo, B. Hegedus, A. Limbeck, Elemental mapping of biological samples by the combined use of LIBS and LA-ICP-MS, J Anal At Spectrom, 31 (2016) 252-258.

[19] D. A. Cremers and L. J. Radziemski, Handbook of Laser-Induced Breakdown Spectroscopy, John Wiley & Sons, Ltd, 2006.

[20] S. Musazzi and U. Perini, Laser-Induced Breakdown Spectroscopy - Theory and Applications, Springer, Italy, 2014.

[21] Q.L. Ma, V. Motto-Ros, W.Q. Lei, M. Boueri, L.J. Zheng, H.P. Zeng, M. Bar-Matthews, A. Ayalon, G. Panczer, and J. Yu, Multi-elemental mapping of a speleothem using laser-induced breakdown spectroscopy, Spectrochim Act B 65 (2010) 707-714.

[22] X. Wang, V. Motto-Ros, G. Panczer, D. De Ligny, J. Yu, J.M. Benoit, J. L. Dussossoy, S. Peuget, Mapping of rare earth elements in nuclear waste glass-ceramic using micro laser-induced breakdown spectroscopy, Spectrochim Act B 87 (2013) 139-146.

[23] V. Motto-Ros, L. Sancey, X.C. Wang, Q.L. Ma, F. Lux, X.S. Bai, G. Panczer, O. Tillement, J. Yu, Mapping nanoparticles injected into a biological tissue using laser-induced breakdown spectroscopy, Spectrochim Acta B, 87 (2013) 168-174.

[24] L. Sancey, V. Motto-Ros, S. Kotb, X. Wang, F. Lux, G. Panczer, J. Yu, O. Tillement, Laser-induced breakdown spectroscopy: a new approach for nanoparticle's mapping and quantification in organ tissue, J Vis Exp, 88 (2014).

[25] L. Sancey, V. Motto-Ros, B. Busser, S. Kotb, J.M. Benoit, A. Piednoir, F. Lux, O. Tillement, G. Panczer, J. Yu, Laser spectrometry for multi-elemental imaging of biological tissues, Sci Rep, 4 (2014) 6065.

[26] L. Sancey, S. Kotb, C. Truillet, F. Appaix, A. Marais, E. Thomas, B. van der Sanden, J.P. Klein, B. Laurent, M. Cottier, R. Antoine, P. Dugourd, G. Panczer, F. Lux, P. Perriat, V. Motto-Ros, O. Tillement, Long-term in vivo clearance of gadolinium-based AGuIX nanoparticles and their biocompatibility after systemic injection, ACS nano, 9 (2015) 2477-2488.

[27] A. Moussaron, S. Vibhute, A. Bianchi, S. Gunduz, S. Kotb, L. Sancey, V. Motto-Ros, S. Rizzitelli, Y. Cremillieux, F. Lux, N.K. Logothetis, O. Tillement, G. Angelovski, Ultrasmall Nanoplatforms as Calcium-Responsive Contrast Agents for Magnetic Resonance Imaging, Small, 11 (2015) 4900-4909.

[28] Y. Gimenez, B. Busser, F. Trichard, A. Kulesza, J.M. Laurent, V. Zaun, F. Lux, J.M. Benoit, G. Panczer, P. Dugourd, O. Tillement, F. Pelascini, L. Sancey, V. Motto-Ros, 3D Imaging of Nanoparticle Distribution in Biological Tissue by Laser-Induced Breakdown Spectroscopy, Sci Rep, 6 (2016) 29936.

[29] D.S. Hill, N.D.P. Robinson, M.P. Caley, M. Chen, E.A. O'Toole, J.L. Armstrong, S. Przyborski, P.E. Lovat, A novel fully-humanised 3D skin equivalent to model early melanoma invasion, Mol Cancer Ther, 14 (2015) 2665-2673.

[30] N.M.G. Walsh, Primary neuroendocrine (Merkel cell) carcinoma of the skin: Morphologic diversity and implications thereof, Hum Pat, 32 (2001) 680-689.

[31] J.T. Mullen, L. Feng, Y. Xing, P.F. Mansfield, J.E. Gershenwald, J.E. Lee, M.I. Ross, J.N. Cormier, Invasive Squamous Cell Carcinoma of the Skin: Defining a High-Risk Group, Ann Surg Oncol, 13 (2006) 902-909.

[32] D. Menut, P. Fichet, J.-L. Lacour, A. Rivoallan, P. Mauchien, Micro-laser-induced breakdown spectroscopy technique: a powerfulmethod for performing quantitative surface mapping on conductive and nonconductive samples, Appl Opt, 42 (2003) 6063-6071.

[33] V. Motto-Ros, E. Negre, F. Pelascini, G. Panczer, J. Yu, Precise alignment of the collection fiber assisted by real-time plasma imaging in laser-induced breakdown spectroscopy, Spectrochim Acta B, 92 (2014) 60-69.

[34] M. Corsi, G. Cristoforetti, M. Hidalgo, S. Legnaioli, V. Palleschi, A. Salvetti, E. Tognoni, C. Vallebona, Application of laser-induced breakdown spectroscopy technique to hair tissue mineral analysis, Appl Opt, 42 (2003) 6133-6137.

[35] M. Alam, D. Ratner Cutaneous Squamous-Cell Carcinoma, N Engl J Med, 344 (2001) 975-983.

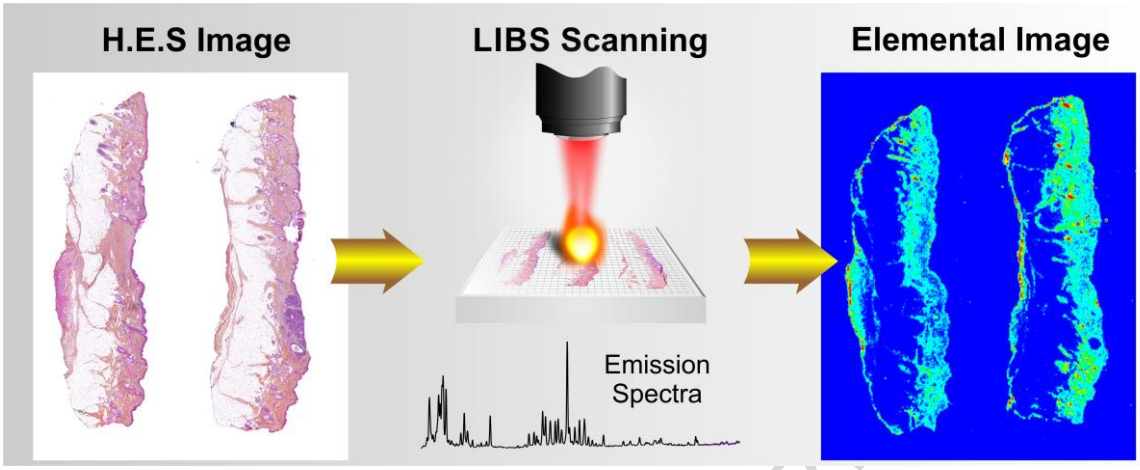

Graphical abstract

Highligths:

- A specific LIBS configuration for imaging human paraffin-embedded samples is proposed.
- High complementarity between LIBS imaging and conventional histopathology is found.
- The most meaningful metal and non-metal elements in medical applications are detected.
- Fast analysis of large healthy and skin tumor biopsies (> 140,000 pixels) is obtain.
- Elemental images of biopsies allow the characterization of tumor lesions.